S01

Proceedings of the 5th International Conference on Inverse Problems in Engineering: Theory and Practice, Cambridge, UK, 11-15th July 2005

INVERSE METHODS FOR DETECTION OF INTERNAL OBJECTS USING MICROWAVE TECHNOLOGY: WITH POTENTIAL FOR BREAST SCREENING

G.G. SENARATNE[1], R.B. KEAM[2], W.L. SWEATMAN[1] and G.C. WAKE[1]
[1] *Institute of Information and Mathematical Sciences, Massey University, Auckland, New Zealand*
e-mail: g.senaratne@massey.ac.nz
[2] *Keam Holdem Associates, 9, Akiraho Street, Auckland, New Zealand*
e-mail: Rickk@keamholdem.com

Abstract - This paper presents one-dimensional and two-dimensional Microwave Inverse Computing methods to detect an internal object using a signal applied from the surface of the host material. The modelling of our application system has been aimed towards the in-vivo detection of a breast tumour, in particular, and to enable the calculation of the tumour size and its distance from the surface of the breast. However, our approach is also applicable for more general foreign object identification.

Complex backscattered electromagnetic waves characterise the relations of the internal properties of the host material. Forward and backscattered signals are used to calculate the impedance and reflection coefficients as a function of the applied microwave frequency. In the study of one-dimensional modelling, we discuss the approach to identifying a foreign object hidden inside the host material and we present a method for computing the distance to the object from the surface of the host. Subsequently a cylindrical coordinate system is used for two-dimensional modelling. A method to compute the size of the object (up to one millimetre in radius) will be discussed. Computation of unknown electrical and non-electrical parameters using front-end microwave application is challenging but it is feasible.

1. INTRODUCTION

A non-destructive method of early stage breast tumour detection can make an important contribution towards the likelihood of successful treatment. The microwave signal we use in this application is harmless because it has a low power and therefore does not harm the normal cells. Screening mammography is the most effective method used for breast cancer detection but it suffers from a number of drawbacks such as; high false-positive and false-negative rates, a possible risk factor, discomfort for the examinee and their difficulty in tolerating breast compression [13, 19]. In our approach the microwave signal applied from the surface of the breast skin requires a minimal compression of the breast for accurate measurements.

Earlier research carried out for internal property measurement of dairy products and food samples have shown that microwave imaging is feasible using a dielectric permittivity profile obtained from a suitable measuring system [20, 7]. Further, ex-vivo measurements taken using the Keam Holden VE2 analyser [9] have shown that a tumour has a significant difference in complex dielectric permittivity to that of healthy breast tissue. Recent studies by Harness *et al.* [4, 5] illustrate the opportunities for active microwave sensing in the breast. X. Li *et al.* [11, 1] have developed a time-domain approach using ultra wideband radar technique to investigate the presence and the location of malignant breast tumours.

We propose non-invasive methods that can be used to identify a very small tumour inside the breast. Our approach analyses the behaviour of the microwave signal and computes the distance from the surface of the host material. The type of signal used in this application is a uniform plane wave which penetrates through the non-homogeneous internal structure. In practice, there are losses due to finite conductivity and lossy dielectric but these are usually very small and can be neglected [3, 17]. The behaviour of the signal with different material properties have led to general eqns which can be obtained from the well-known theory of electromagnetic wave propagation [16, 17]. Those eqns contain information on the electrical and magnetic properties of the internal structure and can be used to develop algorithms to compute the unknown parameters of the internal object. The front-end microwave measurement provides us with the required information which is needed to identify and then to compute these parameters.

The basic model for the microwave measurement system is shown in Figure 1. The measurement system provides the microwave signal to the antenna system which sends the radio signal into the host material. The backscattered signal from the internal structure of the host is received by the same antenna system and sends it back to the measurement system for analysis.

The measured data is then processed using the reconstruction algorithms. There are two main approaches in our study, one is to solve the inverse problem using the reflection coefficient measurements based on the multi-layered plane wave reflection. The other approach is to consider the internal object as a “wave-scatter” and solve the two-dimensional inverse problem in cylindrical coordinates to compute the unknowns. We have begun with simple canonical geometries in order to illustrate the general approach. The one-dimensional study is

straightforward but helps to understand the practical difficulties with accuracy when working with plane wave measurements. It is important because the computed results of the forward and inverse algorithms provide an insight into the subsequent two-dimensional and three-dimensional cases.

The two-dimensional study lays the groundwork for the practical computation of the inverse method using a simple microwave measurement system. Although the forward problem is simple the inverse problem in a two-dimensional application may have practical complications due to the complexity of multiple scattering [12], multipath and diffraction effects in non-homogeneous internal structure of the host material. In order to avoid any incompatibility we treat both forward and inverse problems separately so that our inverse algorithm will be viable for the computation of unknowns based on measured data. The front-end antenna system receives the complex backscattered signal to provide the required data for our inverse algorithm. In both transmitted and received signals, amplitude and phase changes are expected and will be measured a number of times at different frequencies.

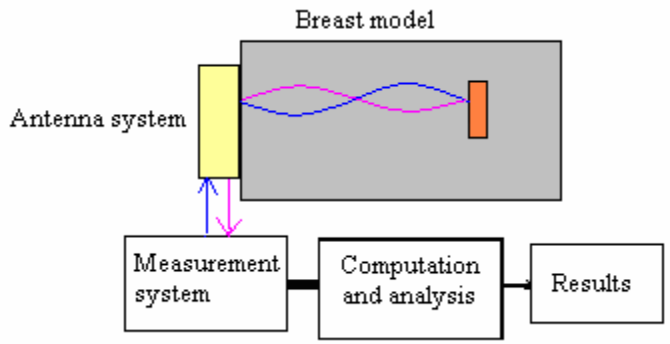

Figure 1. A basic model of the microwave measurement system.

The frequency of the microwave signal must have a constant value during the measurement time but it may be changed to another value for subsequent measurements. In practical application the reflection coefficients are calculated using the measured values of the forward and backward signals through the front-end antenna system.

The reflection coefficient at the front surface of the model for any given profile is given by

$$\Gamma(f) = \frac{Z_{in}(f) - Z_0}{Z_{in}(f) + Z_0} \quad (1)$$

[2] where f represents the frequency of the microwave signal, $Z_{in}(f)$ is the complex electrical impedance into the surface of the breast skin and Z_0 is the complex electrical impedance of the measurement system.

Malignant tumours have increased protein hydration and therefore they have a significant contrast in dielectric properties with normal breast tissue [1, 21]. Because of the changes expected in internal properties, we first consider a simplified model of the internal structure of the breast as thin layers. Then a basic analytical system is constructed for forward and inverse computations to find front-end impedance and the thicknesses of the layers.

2. ONE-DIMENSIONAL STUDY

In the following sections we analyse the time and space dependence of the microwave signal within the application model. The plane wave reflection model is shown in Figure 2.

The internal structure of the host material is represented using a number of regions, each of which is homogeneous. In particular, we assume that the electrical properties are constant over each of these regions. For the one-dimensional model, the regions are a number of thin rectangular layers which have been cascaded to form the host material.

The layers inside the model are specified with individual material properties. These are permittivity ε, permeability μ and conductivity σ and they characterise the media with electric flux, magnetic flux and the electric current, respectively. When the microwave signal is applied from the front it penetrates through the layers and, if the properties of any two layers differ from each other, it reflects back from the boundary between them. Similarly, looking from the electrical view point, it can be observed that each of these layers must have individual impedances in the presence of uniform plane waves. In order to find the reflection from the surface of the host it is necessary to perform a series of impedance transformations at the layer boundaries.

The impedance transformation towards the front end can be seen as a belt with n cascaded strips, looking from the front, as shown in Figure 2. We consider the host internal structure to be loss less ($\sigma = 0$) for the electromagnetic waves and therefore that the wave propagation depends only upon the complex value of the propagation constant [8].

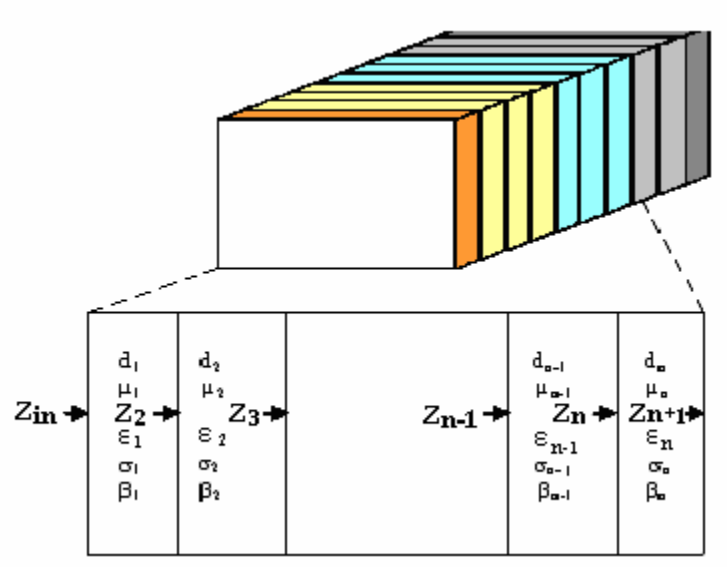

Figure 2. Plane wave reflection model.

(a) Impedance transformation

The front-end impedances of the layers are indicated as $Z_{(.)}$ (looking from the front) and the first and last layer impedances are taken as Z_{in} and Z_{n+1} respectively. For simplicity, in the reminder of this paper the magnetic permeability μ is assumed to be unity, but this is not a restriction for this application. The recursive eqn to find the electrical impedance [16] at the front of the n^{th} layer of the model that has a width of d_n is

$$Z_n(f) = \eta_n(f).\frac{Z_{n+1} + \eta_n(f)\tanh[\beta_n(f)d_n]}{\eta_n(f) + Z_{n+1}\tanh[\beta_n(f)d_n]} \tag{2}$$

where $\eta_n(f)$ is the intrinsic or characteristic impedance of the n^{th} layer given by,

$$\eta_n(f) = \frac{\eta_0}{\sqrt{\varepsilon_n(f)}} \tag{3}$$

and η_0 is the intrinsic impedance in a vacuum and is approximately equal to 377 Ohms. The ε_n is the relative permittivity of the n^{th} layer. Here, $\beta_n(f)$ represents the phase constant of the n^{th} layer given by

$$\beta_n(f) = \frac{2\pi f\sqrt{[\varepsilon_n(f)]}}{c} \tag{4}$$

where c is the velocity of light given as approximately 3×10^8 m/s and f is the frequency of the microwave signal.

Using eqn (2), the front-end impedance of any layer can be calculated when given the characteristic impedance and the propagation constant of that layer and the load impedance of the succeeding layer. Starting with the known impedance of the last layer (the deepest layer of the model), the layer impedances can be computed from layer to layer backward up to the surface of the front layer. Finally this result is used to compute the reflection coefficient using eqn (1).

If there are three layers having thicknesses of d_{n-1}, d_n and d_{n+1} the front-end impedance of the $(n\text{-}1)^{th}$ layer at the frequency f_i can be found by substituting Z_n in the eqn that is obtained for Z_{n-1} using the eqn (2). Then at frequency f_i,

$$Z_{i,n-1} = \eta_{i,n-1}\left[\frac{Z_{i,n+1}\left[\eta_{i,n} - \eta_{i,n-1}\tan(\beta_{i,n}d_n)\tan(\beta_{i,n-1}d_{n-1})\right] + \eta_{i,n}j[\eta_{i,n}\tan(\beta_{i,n}d_n) + \eta_{i,n-1}\tan(\beta_{i,n-1}d_{n-1})]}{Z_{i,n+1}j[\eta_{i,n-1}\tan(\beta_{i,n}d_n) + \eta_{i,n}\tan(\beta_{i,n-1}d_{n-1})] + \eta_{i,n}[\eta_{i,n-1} - \eta_{i,n}\tan(\beta_{i,n}d_n)\tan(\beta_{i,n-1}d_{n-1})]}\right] \tag{5}$$

where Z_i, β_i and η_i represent the front–end impedance, phase constant and characteristic impedance, respectively (at the frequency f_i) and $j = \sqrt{-1}$.

Using the above eqn we can obtain two different eqns using two frequencies (i=1 and i=2) and those eqns can be used to find the two unknowns in Z_n and Z_{n-1} layers.

Equation (5) calculates the front-end impedance without knowing the front-end impedance Z_n of the middle layer. Similarly this procedure can be continued up to the first layer of our model to calculate the front-end

impedance, Z_{in} *(f).* The final eqn of this process would be a large and complicated eqn which has a number of unknowns. We can obtain *i* eqns for *i* frequencies and those eqns can be used to find the *i* unknowns.

If the reflection coefficients are known from the measurement system then we can find the front-end impedance of the host material and this can be used to find the unknowns (this will be explained below).

(b) Layer thickness calculation

Using the microwave antenna system we can measure the front-end impedance, Z_{in} *(f)* of the host material. Suppose we know the front-end impedance by practical measurement. Then the new task is to find the distance to the object from the surface of the host. The total distance is the sum of the individual widths of each layer. This can be calculated using inverse eqns derived from the eqn (5).

If we take the three layers, the distance to the $(n\text{-}1)^{th}$ layer from the $(n+1)^{th}$ layer can be obtained from

$$d_{n-1}\beta_{n-1} = \tan^{-1}\left[\frac{\eta_{n-1}\eta_n(Z_{n+1}-Z_{n-1}) + j.\tan(\beta_n d_n)(\eta_{n-1}\eta_n^{\,2} - Z_{n+1}Z_{n-1})}{j.\eta_n(Z_{n+1}Z_{n-1} - \eta_{n-1}^{\,2}) - \tan(\beta_n d_n)(Z_{n-1}\eta_n^{\,2} - Z_{n+1}\eta_{n-1}^{\,2})}\right]. \quad (6)$$

By following the above procedure, we can find a similar eqn for even more than three layers. In the eqn (6), we have two unknowns, d_{n-1} and d_n. For simplicity we assume Z_{n+1} =0. Then using eqn (6) we obtain a general eqn as

$$F(f_i, d_{n-1}, d_n) = j[\eta_{n-1}(f_i)]^2 \tan[\beta_{n-1}(f_i)d_{n-1}] + Z_{n-1}[\eta_n(f_i)]\tan[\beta_{n-1}(f_i)d_{n-1}]\tan[\beta_n(f_i)d_n] - Z_{n-1}[\eta_{n-1}(f_i)] + j.[\eta_{n-1}(f_i)\eta_n(f_i)\tan[\beta_n(f_i)d_n] = 0 \quad (7)$$

where f_i is the microwave frequency applied at each measurement, and *i*=1,2,....,*m*.

As there is more than one unknown, it is not possible to obtain a direct solution using a single eqn. Therefore we obtain *m* eqns from *m* trials each applying a different frequency into the system. In order to find the unknowns we use an algorithm based on Newton's iterative method [10].

Let our unknowns be the thicknesses of the layers. Then the set of eqns are;

$$F(X) = \begin{bmatrix} F_1(d_1, d_2, ..., d_n) = 0 \\ F_2(d_1, d_2, ..., d_n) = 0 \\ \vdots \\ F_n(d_1, d_2, ..., d_n) = 0 \end{bmatrix}. \quad (8)$$

We form the $n \times n$ Jacobian matrix of the above system of eqns. That is;

$$J = [J_{k,l}] \quad (9)$$

where $J_{k,l} = \partial F_k / \partial d_l$ and $k, l = 1, 2, ..., n$.

Using the initial guess for $X^{(0)} = (d_1(g), d_2(g), ... , d_n(g))^T$, we carry out a nonlinear multidimensional Newton's method [14] to search for the solution to $F(X) = 0$. The solution of the above system often needs several iterations and the number of these mainly depends upon the number of unknowns and the value of the initial guess.

(c) Results of the one-dimensional model

(i) Front-end Impedance

Using eqn (2), the front-end impedance of 10 layers was calculated recursively. Starting with the last layer, Z_{n+1}, the calculation is carried out from layer to layer backward up to the first layer, Z_1. The simulation results have been plotted in Figure 3. The plot (1) is for the layers having electrical properties similar to normal breast tissue. The plot (2) is similar except that the last layer's electrical properties are set to be similar to those of a breast tumour.

There is a significant difference in front-end impedance when the permittivity, the dielectric constant, of the last layer is 50 rather than 10 as in the other layers. Therefore with our detection system there should be a high probability of identifying an internal object with significantly different material properties to its surroundings.

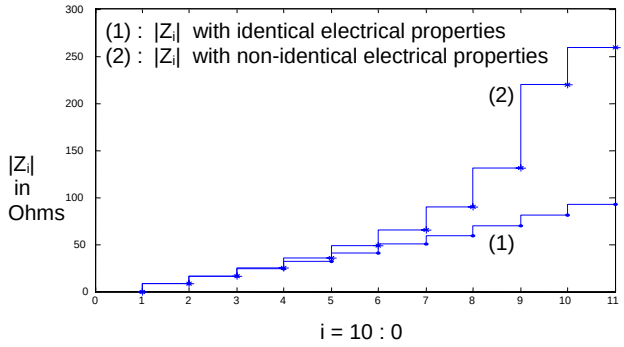

Figure 3. Plot of the layers' front impedance.

(ii) Distance calculation

Finding the layer thicknesses is important because the arithmetic addition of each of these thicknesses will give the distance from the surface to the boundary of the layer of our interest. For an example, we tested our algorithm by computing the layer thicknesses of two layers (n=2) of our model. Using eqn (5) we first calculated the front-end impedances of the $(n\text{-}1)^{\text{th}}$ layer for two different frequencies. The layer thicknesses of the n^{th} layer and the $(n\text{-}1)^{\text{th}}$ layer are taken as 0.002 and 0.004 metres respectively. Now, by knowing the values of $Z_{1,n-1}$ and $Z_{2,n-1}$ for two different frequencies, we estimate the values d_1 and d_2 using two eqns of the form of eqn (7). That is

$$F(X) = \begin{bmatrix} F_1(d_1, d_2) = 0 \\ F_2(d_1, d_2) = 0 \end{bmatrix} . \tag{10}$$

In full,

$$\begin{bmatrix} j[\eta_{1,n-1}(f_1)]^2 \tan[\beta_{1,n-1}(f_1))d_{n-1}] + Z_{1,n-1}[\eta_{1,n}(f_1)]\tan[\beta_{1,n-1}(f_1)d_{n-1}]\tan[\beta_{1,n}(f_1)d_n] \\ \qquad - Z_{1,n-1}[\eta_{1,n-1}(f_1)] + j.[\eta_{1,n-1}(f_1)\eta_{1,n}(f_1)\tan[\beta_{1,n}(f_1)d_n] \\ j[\eta_{2,n-1}(f_2)]^2 \tan[\beta_{2,n-1}(f_2)d_{n-1}] + Z_{2,n-1}[\eta_{2,n}(f_2)]\tan[\beta_{2,n-1}(f_2)d_{n-1}]\tan[\beta_{2,n}(f_2)d_n] \\ \qquad - Z_{2,n-1}[\eta_{2,n-1}(f_2)] + j.[\eta_{2,n-1}(f_2)\eta_{2,n}(f_2)\tan[\beta_{2,n}(f_2)d_n] \end{bmatrix} = \begin{bmatrix} 0 \\ 0 \end{bmatrix} . \tag{11}$$

The solution for $d_1$and d_2 was computed using Newton's method [10] in MATLAB and the results are plotted in Figure 4 (Newton's method is further explained in the two-dimensional study.). The two graphs show that the approximations to d_1 and d_2 in F_1 and F_2 rapidly approach the exact values of d_1=0.002 metres and d_2=0.004 metres.

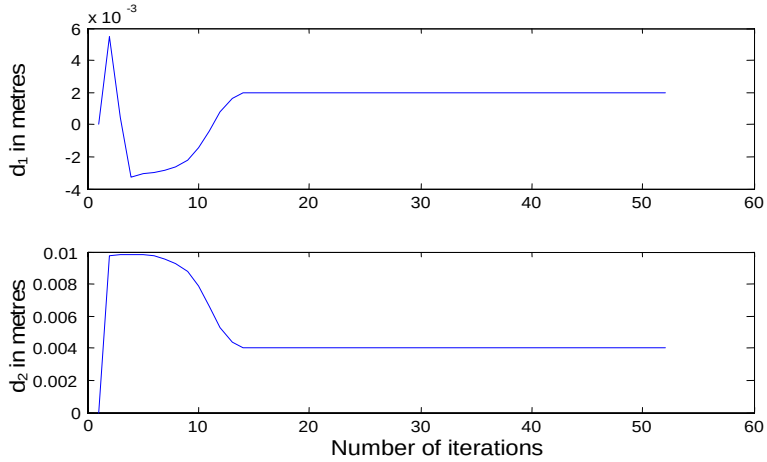

Figure 4. Computed results of layer thicknesses, d_1 and d_2.

3. TWO-DIMENSIONAL STUDY

In this approach we consider the internal object as a conducting cylinder which has a radius in millimetres. The microwave signal application system is almost the same as Figure 1 but the model of the host material is different from the one-dimensional case. The two-dimensional model with cylindrical coordinates is shown in Figure 5. This model analyses the behaviour of the microwave signal propagation and scattering effect at the boundary of the cylinder (the circle with the radius a represents the cylinder in the model).

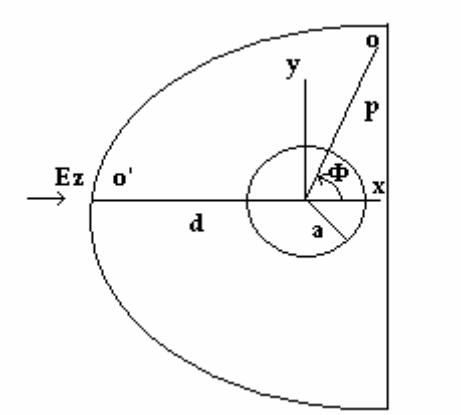

Figure 5. Two-dimensional model with cylindrical coordinates.

We consider this to be a single scatter problem and construct the electromagnetic wave eqns for the forward and scattered fields using the solutions to the scalar Helmholtz eqn [6]. Our discussion of the two-dimensional model is restricted to the conducting cylinder, here the extension to the case of a non-conducting cylinder having dielectric with the parameters μ and ε similar to those of a breast tumour can be developed as in [15] and [18]. In this latter case the boundary conditions of the normal and scattering fields of the cylinder will be based on the wave impedance that we discussed in the one-dimensional model.

A plane wave incident upon the host material can be expressed in terms of cylindrical waves [6]. The incident wave at the host material is z-polarised and travelling in the *x* direction as shown in Figure 5. The forward incident wave of frequency *f* is

$$E_z^{\,i}(f) = E_0 e^{-jkx} = E_0 e^{-jkp\cos\phi} \tag{12}$$

where *p* is the radial distance from the centre of the cylinder, ϕ is the angle with respect to the *x* direction and *k* is the wave number of the medium given by,

$$k = \frac{2\pi f\sqrt{\mu\varepsilon}}{c} \quad . \tag{13}$$

The wave number is expressed in terms of ε the permittivity of the medium, μ the permeability of the medium and *c* the velocity of light.

The wave is finite at the origin and periodic in ϕ with period 2π. Therefore the solution to the eqn (12) can be found as,

$$E_z^{\,i}(f) = E_0 \sum_{n=-\infty}^{\infty} j^{-n} J_n(kp) e^{jn\phi} \tag{14}$$

where J_n is the Bessel function [22] of the first kind.

For the outward-travelling waves due to scattering at the cylinder boundaries, the scattered field is

$$E_z^{\,s}(f) = E_0 \sum_{n=-\infty}^{\infty} j^{-n} a_n H_n^{(2)}(kp) e^{jn\phi} \tag{15}$$

where $H_n^{(2)}$ is the Hankel function [6, 22] of second kind.

The total field is the sum of the incident and scattered field, that is,

$$E_z(f) = E_z^{\,i}(f) + E_z^{\,s}(f) \tag{16}$$

Considering the boundary condition of the cylinder, the total field at the point o given by eqn (16) can be re-written using eqns (14) and (15).

$$E_z(f) = E_0 \sum_{n=-\infty}^{\infty} j^{-n} \left[J_n(kp) - \frac{J_n(ka)}{H_n^{(2)}(ka)} . H_n^{(2)}(kp) \right] e^{jn\phi} \quad . \tag{17}$$

Equation (17) is the general wave eqn that can be used to find the total field at any point o in our two-dimensional model. Now, suppose the point o is rotated to the point o' where o' lies along the *x* axis. If we consider this model for the breast tumour case then the distance o' is the distance to the centre of the tumour from the surface of the breast. The eqn after rotating the point o into point o' is

$$E_z(f) = E_0 \sum_{n=-\infty}^{\infty} j^{-n} \left[J_n(kd) - \frac{J_n(ka)}{H_n^{(2)}(ka)} . H_n^{(2)}(kd) \right] (-1)^n \quad . \tag{18}$$

The computational cost of the inverse process depends on the number of arithmetic operations required to calculate (18) accurately. It can be reduced by combining terms with positive and negative values of *n*. The new eqn is

$$E_z(f) = E_0 \sum_{n=1}^{\infty} \left[J_n(kd) - \frac{J_n(ka)}{H_n^{(2)}(ka)} . H_n^{(2)}(kd) \right] 2j^n + E_0 \left[J_0(kd) - \frac{J_0(ka)}{H_0^{(2)}(ka)} . H_0^{(2)}(kd) \right]. \qquad (19)$$

Equation (19) is the general eqn we use to find the unknowns for the two-dimensional model. Using a similar approach to that used in the one-dimensional case, $E_z(f)$ can be measured and then eqn (19) may be numerically inverted in order to determine *a* and *d.*

Results of the two-dimensional study

In the forward problem *a* and *d* are known at a single location of the cylinder and the amplitude values of the scattering field at each frequency have to be computed. In the inverse problem the field quantity at the receiver is known by measurement and *a* and *d* are the unknowns.

In order to find the two unknowns *a* and *d*, we use eqn (19) to obtain two different eqns by applying two different frequencies. In the practical situation we can measure $E_z(f)$ for these two frequencies and proceed to compute the two unknowns. In the analytical study we used reasonable values for *a* and *d* (*a*=0.002metres and *d*=0.04metres) to calculate two $E_z(f)$ values. As there are Bessel and Hankel functions inside the summation of the eqn, it is necessary to handle eqn (19) carefully to obtain the correct answer for $E_z(f)$.

Again we have two eqns of the form

$$E_{1,z}(a, d) = 0$$
$$E_{2,z}(a, d) = 0 \qquad (20)$$

where we now use the subscripts 1 and 2 to indicate two different frequencies.

Solution of the inverse problem leads to the internal object reconstruction and the routine is summarised as follows.

We start from an initial approximation to our unknowns, $X^{(0)} = (a_0, d_0)^T$. Subsequent improvements to this approximation $X^{(N)} = (a_N, d_N)^T$, N=1,2,…, are obtained by the following steps:

1). Compute the field component based on the incident and the scattered field. The circular boundary of the cylinder is the cause of the potential scatter and the angle ϕ determines the receiver location for the measuring system. The wave number *k* is frequency dependent and there exists a field component for each frequency.

2). Form the difference of the field vectors by subtracting the calculated field components from the measured electric fields.

3). Construct the $n \times n$ Jacobian matrix $J_{l,m}$, l, m = 1, 2,…, n, which is necessary in Newton's method to find the minimum difference in '2' above.

4). Obtain the correction vector and form the implicit function for the vector $X^{(N)}$ to update the computed values of unknowns in the vector $X^{(N-1)}$ [10, 14].

5). Repeat the steps 1-4 until the vector $X^{(N)}$ satisfies some suitable stopping criteria.

Following the above procedure the two unknowns were computed. The result is shown in Figure 6. The two graphs show that the approximations to *a* and *d* in E_1 and E_2 rapidly approach the exact values of *a*=0.002 metres and *d*=0.04 metres.

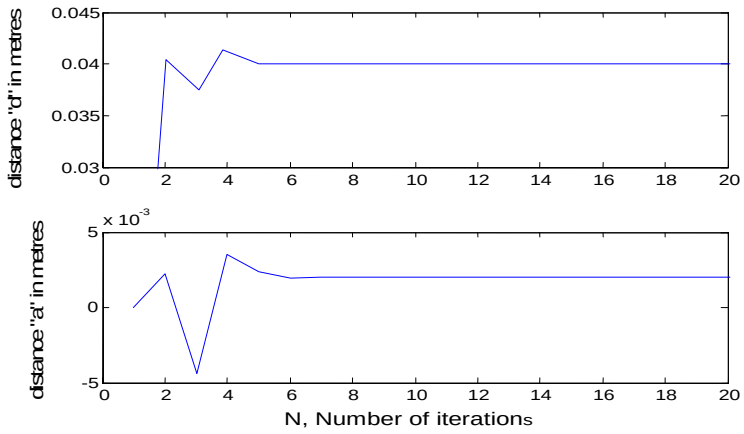

Figure 6. Plot of calculated values of '*a*' and '*d*' using Newton's method.

The plot of E_1 and E_2 versus number of iterations is shown in Figure 7. Both E_1 and E_2 converge towards zero as a and d approach 0.002 metres and 0.04 metres, respectively (approximately after 12 iterations).

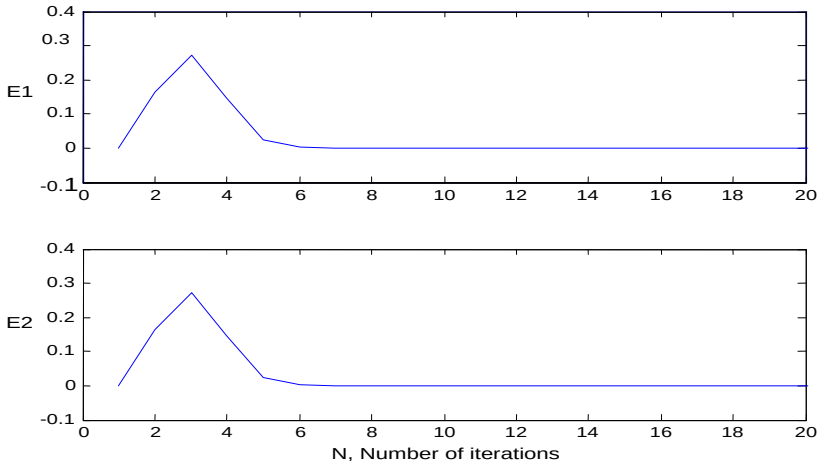

Figure 7. Plots of $E_1$and E_2 versus number of iterations.

When we determine $E_z(f)$, we use eqn (19), truncating the series at successively larger values of n until we obtain a steady value for $E_z(f)$. The value of n will depend on the values of frequency, distance d, radius a and the electrical parameters of the medium. Care must be taken when testing for convergence of eqn (19) since the solution oscillates with respect to n. The accuracy of the initial guess can also be a limitation.

We carried out a number of simulations to test our inverse algorithm for convergence. First, using the forward method, the values of $E_z(f)$ and $E_z(f)$ were calculated for the values of a and d equal to 0.002 metres and 0.04 metres respectively. Those results were used in our inverse algorithm to test for the convergence using a range of initial (guess) values of a and d. The selected range starts from a=0.001 metres and d=0.03 metres and changed by 0.0002 and 0.002 up to a=0.003 metres and d=0.05 metres respectively. Every pair of initial values were tested separately and the number of iterations, N, required for convergence is counted after every simulation and the result is shown in Figure 8. The x and y axes represent the initial values of a and d, respectively. Every grid point has a corresponding set of a and d initial values and the number of iterations (N) required for the convergence can be found at the grid point.

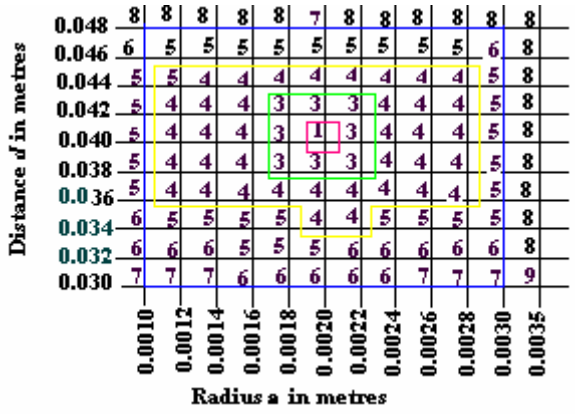

Figure 8. Result of the simulations for convergence using different initial values of a and d.

When the initial values are far away from the true values we require a large number of iterations and furthermore there exists a range beyond which we cannot expect any accuracy in the convergence. In our test, a and d can vary up to $\pm 50\%$ and $\pm 25\%$ from their actual values, respectively. For our example we found a=0.001:0.003 and d=0.03:0.48 is safe range for convergence with a reasonable number of iterations. We suggest that in general 20 iterations are used in order to determine whether the process is within a safe range

before restarting the iteration process with alternative starting values for *a* and *d*. It is important to display the result with double precision in order to identify the exact solution.

Table 1: Result of the error analysis.

Measurement error	Error in *a*	Error in *d*
1%	2.1%	0.005%
2%	5.1%	0.125%
3%	10.5%	0.16%
5%	18.5%	0.31%
7.5%	29.5%	0.41%
10%	41.5%	0.54%

We carried out an error analysis to study the robustness of the inverse computation method with respect to measurement errors in the forward system. We added errors into $E_z(f_1)$ and $E_z(f_2)$ and simulated to find the corresponding errors in *a* and *d* values. Those values are tabulated in Table 1. The percentage error in *a* is quite large with large measurement errors. We should note that our original value of *a* is small (*d* is twenty times larger than *a*) compared to *d*. However in general, *d* is less sensitive to measurement errors than *a*.

In practice some form of calibration could be performed to reduce the influence of measurement error. This could consist, for example, of normalising the measurement data to measured data taken where it is known that there are no scattering objects present.

CONCLUSIONS

The microwave inverse computing method we used in this study has demonstrated how we can use the differences in microwave signal behaviour at a high contrast in material properties. In the one-dimensional model a layer of high permittivity equivalent to that of a breast tumour is capable of providing a significant difference in front-end impedance. Therefore by the reflection coefficients obtained in microwave in-vivo measurements, identification of a breast tumour should be feasible. Similarly the algorithm developed for three layers indicates that the computation of the distance to the cancer from the breast skin surface will be possible.

Two-dimensional study of the microwave inverse computing method has proved its capability of estimating the tumour distance in the breast model. Apart from that, it can estimate the size of the tumour by calculating the radius of the cylinder of our model. The tests carried out for a range of initial values have demonstrated that our algorithm can detect a millimetre size internal object and estimate the radius and the distance from the surface of the host.

Further work will use 3-dimensional modelling with a similar approach. This will provide more capability to compute accurate dimensions of a breast tumour. We plan to construct an image profile to identify an internal object using in-vivo microwave measurements.

Acknowledgement

We are grateful to ***Technology New Zealand*** for providing a TIF fellowship for PhD study on Microwave signal processing for breast cancer detection. We thank referees for their helpful comments.

REFERENCES

1. E.J. Bond, X. Li, S. C. Hagness and B.D.V. Veen, Microwave imaging via space-time beam forming for early detection of breast cancer. *IEEE Trans. Antennas Propagation* (2003) **51**, 1690-1705.

2. K.R. Demarest, *Engineering Electromagnetic*, Prentice Hall, Inc. 1998, pp. 366-370.

3. E.C. Fear and M.A. Stuchly, Microwave detection of breast cancer. *IEEE Trans. Microwave Theory Techniques* (2000) **48**, 1854-1863.

4. C.G. Hagness, A. Taflove and J.E. Bridges, Three dimensional FDTD analysis of a pulsed microwave conforcal system for breast cancer detection. *IEEE Trans. Antennas Propagation* (1999) **47**, 783-791.

5. C.G. Hagness, A. Taflove and J.E Bridges, Two dimensional FDTD analysis of a pulsed microwave conforcal system for breast cancer detection: Fixed-focus and antenna array sensors. *IEEE Trans. Biomed. Eng.* (1998) **45**, 1470-1479.

6. R.F. Harrington, *Time-Harmonic Electromagnetic Fields*, McGraw-Hill, New York, 1961, pp. 198-238.

7. R.B. Keam and G.G. Senaratne, Microwave moisture and salt measurement for the New Zealand dairy industry, *Proc. of fifth ISEMA conference on Wave Interaction with Water and Moisture Substances*, March 2003, pp.369-376.

8. R.B. Keam, J.R. Holdem and J.A. Schoonees, Soil moisture estimation from surface measurements at multiple frequencies. *Aust. J. Soil Res*. (1999) **37**, 1107-1121.

9. R.B. Keam, G.G. Senaratne and R. Pochin, One-dimensional propagation difference between tumour and healthy breast tissue at 2 GHz, *Proc. of New Zealand National Conference on Non Destructive Testing,* 2004, pp. 21-25.

10. D. Kincaid and W. Cheney, *Numerical Analysis*: *Mathematics of Scientific Computing*, 3rd edn., Brooks/Cole, 2002, pp. 81-90.

11. X. Li, S.K. Davis, S.C. Hagness, D.W. V. Weide and B.D.V. Veen, Microwave imaging via space-time beam forming: experimental investigation of tumour detection in multilayer breast phantoms. *IEEE Trans. Microwave Theory Techniques* (2004) **52**, 1856-1865.

12. Q.H. Liu, Z.Q. Zhang, T.T. Wang, J.A. Bryan, G.A. Ybarra, L.W. Nolte and W.T. Joines, Active microwave imaging I: 2-D forward and inverse scattering methods. *IEEE Trans. Microwave Theory Techniques* (2002) **50**, 123-133.

13. M. Meaney, M.W. Fanning, D.Li, S.P. Poplack and K.D. Paulsen, A clinical prototype for active microwave Imaging of the Breast. *IEEE Trans. Microwave Theory Techniques* (2000) **48,** 1841-1853.

14. P.M. Meaney, K.D. Paulsen and T.P. Ryan, Two-dimensional hybrid element image reconstruction for TM illumination. *IEEE Trans. Antennas Propagation* (1995) **43**, 239-247.

15. G.P. Otto and W. Chew, Microwave inverse scattering-local shape function imaging for improved resolution of strong scatters. *IEEE Trans. Microwave Theory Techniques* (1994) **42**, 137-141.

16. D.M. Pozar, *Microwave Engineering,* 3rd edn., John Wiley & Sons, New York, 2005, pp. 49-86.

17. S. Ramo, J.R. Whinnery and T.V. Duzer, *Field and Waves in Communication Electronics*, 3rd edn., John Wiley & Sons, New York, 1994, pp. 213-250 and 283-287.

18. I.T. Rekanos and T.D. Tsiboukis, An inverse scattering technique for microwave imaging in binary objects. *IEEE Trans. Microwave Theory Techniques* (2002) **50**, 1439-1441.

19. A. Rosen, M.A. Stuchly and A.V. Vorst, Application of RF/Microwaves in medicine. *IEEE Trans. Microwave Theory Techniques* (2002) **50**, 963-974.

20. G. Senaratne and S.C. Mukhopadhyay, Investigation of the interaction of planar electromagnetic sensor with dielectric materials at radio frequencies. *Proc. of fifth ISEMA Conference on Wave Interaction with Water and Moisture Substances,* New Zealand, March 2003, pp.95-99.

21. A.J. Surowiec, S.S. Stuchly, J.R. Barr and A. Swarup, Dielectric properties of the breast carcinoma and the surrounding tissues. *IEEE Trans. Biomed. Eng.* (1988) **35**, 257-263.

22. G.N. Watson, *Theory of Bessel Functions*, Cambridge University Press, 1962, pp. 14-83.